# Preoperative 11C-Methionine PET-MRI in Pediatric Infratentorial Tumors

Pierre-Aurélien Beuriat, Anthime Flaus, Aurélie Portefaix, Alexandru Szathmari, Marc Janier, Marc Hermier, Sylvie Lorthois-Ninou, Christian Scheiber, Sibel Isal, Nicolas Costes, et al.

OPEN

# Preoperative $^{11}$C-Methionine PET-MRI in Pediatric Infratentorial Tumors

*Pierre-Aurélien Beuriat, MD, PhD,*† Anthime Flaus, MD, PhD,†‡§ Aurélie Portefaix, MD, MSc,||¶ Alexandru Szathmari, MD, PhD,* Marc Janier, MD, PhD,†‡ Marc Hermier, MD, PhD,** Sylvie Lorthois-Ninou, MD,†† Christian Scheiber, MD, PhD,†‡ Sibel Isal, MD,‡ Nicolas Costes, PhD,‡‡ Ines Merida, PhD,‡‡ Sophie Lancelot, PharmD, PhD,§‡‡ Alexandre Vasiljevic, MD, PhD,§§ Pierre Leblond, MD, PhD,|||| Cécile Faure Conter, MD,|||| Clarisse Saunier, MSc,|| Behrouz Kassai, MD, PhD,||¶ Matthieu Vinchon, MD, PhD,* Federico Di Rocco, MD, PhD,*† and Carmine Mottolese, MD, PhD**

**Purpose:** MRI is the main imaging modality for pediatric brain tumors, but amino acid PET can provide additional information. Simultaneous PET-MRI acquisition allows to fully assess the tumor and lower the radiation exposure. Although symptomatic posterior fossa tumors are typically resected, the patient management is evolving and will benefit from an improved preoperative tumor characterization. We aimed to explore, in children with newly diagnosed posterior fossa tumor, the complementarity of the information provided by amino acid PET and MRI parameters and the correlation to histopathological results.

**Patients and Methods:** Children with a newly diagnosed posterior fossa tumor prospectively underwent a preoperative $^{11}$C-methionine (MET) PET-MRI. Images were assessed visually and semiquantitatively. Using correlation, minimum apparent diffusion coefficient ($ADC_{min}$) and contrast enhancement were compared with MET $SUV_{max}$. The diameter of the enhancing lesions was compared with metabolic tumoral volume. Lesions were classified according to the 2021 World Health Organization (WHO) classification.

**Results:** Ten children were included 4 pilocytic astrocytomas, 2 medulloblastomas, 1 ganglioglioma, 1 central nervous system embryonal tumor, and 1 schwannoma. All lesions showed visually increased MET uptake. A negative moderate correlation was found between $ADC_{min}$ and $SUV_{max}$ values ($r = -0.39$). Mean $SUV_{max}$ was 3.8 (range, 3.3–4.2) in WHO grade 4 versus 2.5 (range, 1.7–3.0) in WHO grade 1 lesions. A positive moderate correlation was found between metabolic tumoral volume and diameter values ($r = 0.34$). There was no correlation between $SUV_{max}$ and contrast enhancement intensity ($r = -0.15$).

**Conclusions:** Preoperative $^{11}$C-MET PET and MRI could provide complementary information to characterize pediatric infratentorial tumors.

**Key Words:** amino acid PET, diffusion-weighted imaging, children, neuro-oncology, posterior fossa tumor, hybrid imaging, precision oncology

(*Clin Nucl Med* 2024;49: 381–386)

MRI is the main imaging modality to characterize pediatric brain tumors. MRI can determine the type of posterior fossa tumor in children, especially when advanced techniques, such as diffusion-weighted imaging and apparent diffusion coefficient (ADC) maps, MR spectroscopy (MRS), and perfusion-weighted imaging, are added. However, MRI can lack specificity: ADC characteristics may overlap between the tumor types and grades,[1] and MR spectra can be degraded by hemorrhage, calcifications, or vessels. Furthermore, the diagnosis of some pseudotumoral lesions that do not require surgery may remain challenging.

PET imaging using amino acid analogs, for example, [$^{11}$C-methyl]-methionine ($^{11}$C-MET), *O*-(2-[$^{18}$F]fluoroethyl)-L-tyrosine ($^{18}$F-FET), and 3,4-dihydroxy-6-[$^{18}$F]fluoro-L-phenylalanine ($^{18}$F-DOPA), can provide additional information. The uptake of amino acid analogs in glioma is related to proliferation and neovascularization, and correlates with the expression of the nuclear antigen Ki-67 and microvessel density.[2] Information obtained through amino acid analog PET imaging could improve the differentiation between tumors and pseudotumoral lesions, predict the histological grade, define the tumor extension, and improve prognosis prediction in adults and children,[3–6] which can provide complementary information to MRI.

Hybrid imaging, using a PET-MRI scanner, appears particularly suitable for children[7–9]; in brain tumors, it is useful to avoid 2 examinations,[10] and therefore a potential need for general anesthesia.[11] In addition, compared with PET/CT, it allows a lower radiation exposure,[12,13] which is particularly important in children.

Although symptomatic posterior fossa tumors are typically resected, it has been reported that posterior fossa surgery may have a critical impact on the sensorimotor and cognitive outcomes of children.[14,15] The current management of brain tumors in children is evolving due to an improved understanding of the molecular mechanisms, even though biomarkers are lacking. The complementary information provided by PET and MRI, for example, SUV and ADC, could improve tumor characterization and, indirectly, the use

From the *Department of Pediatric Neurosurgery, Hôpital Femme Mère Enfant, Hospices Civils de Lyon; †Faculté de Médecine Lyon Est, Université Claude Bernard Lyon 1; ‡Department of Nuclear Medicine, Hospices Civils de Lyon; §Lyon Neuroscience Research Center; INSERM U1028/CNRS UMR5292; ||EPICIME-CIC 1407 de Lyon, Inserm, Département d'Épidémiologie Clinique, Hospices Civils de Lyon; ¶CNRS, UMR 5558, Laboratoire de Biométrie et Biologie Evolutive, Université Lyon 1; **Department of Neuroradiology, Hôpital Neurologique et Neurochirurgical P. Wertheimer, Hospices Civils de Lyon; ††Department of Pediatric Radiology, Hôpital Femme Mère Enfant, Hospices Civils de Lyon; ‡‡CERMEP-Life Imaging; §§Department of Pathology and Neuropathology, Hospices Civils de Lyon; and ||||Institut d'Hématologie et d'Oncologie Pédiatrique (IHOPe), Centre Léon Bérard, Lyon, France.

Received for publication November 21, 2023; revision accepted January 30, 2024.

P.-A.B. and A.F. contributed equally to this work and share the first authorship.

Conflicts of interest and sources of funding: The authors have no conflicts of interest to declare. P.-A.B. received funding from the Hospices Civils de Lyon Foundation, Banque Populaire AURA, and the Flavien Foundation for their financial support.

Correspondence to: Anthime Flaus, MD, PhD, Department of Nuclear Medicine, Hospices Civils de Lyon, 32 Avenue du Doyen Jean Lépine, 69677 Lyon Cedex, France. E-mail: anthime.flaus@chu-lyon.fr.



ISSN: 0363-9762/24/4905–0381

DOI: 10.1097/RLU.0000000000005174

of molecular targeted therapies.[16] Moreover, PET-MRI information could allow to avoid a high-risk surgical procedure in some children.[8,17]

Integrated analysis of amino acid PET and MRI data is limited to diffuse astrocytic tumors and diffuse midline glioma in children. A significant negative correlation between MRI minimum ADC ($ADC_{min}$), a marker of tumor cellularity, and amino acid uptake[18,19] was found, whereas a study in high-grade brain tumors in adults did not report it.[20] The aim of the present study was to explore the complementarity of the information provided by amino acid PET and MRI parameters, as well as their correlation with histopathologic results, in posterior fossa tumors in children.

## PATIENTS AND METHODS

The study complied with the principles of the Declaration of Helsinki and was approved by the institutional review board (CPP Sud Ouest et Outre Mer II 2019/09/06) and the national agency for the safety of medicines and health products (ANSM 2019/07/25). This study was registered on clinicaltrials.gov (NCT 03977896). All legal guardians gave prior written informed consent for the participation of children in the study.

### Patients

The inclusion criteria were as follows: being admitted to the pediatric neurosurgical department of the Hospices Civils de Lyon between 2019 and 2021 for a newly diagnosed posterior fossa tumor, age ≥5 years and <18 years, consent of the legal guardians, no pregnancy, and no contraindication to contrast-enhanced (CE) PET-MRI. The exclusion criteria were as follows: PET-MRI not performed within 7 days after admission and medical condition not suitable for the examination.

### PET-MRI Acquisition and Image Reconstruction

$^{11}$C-MET was synthetized as previously described.[21] All patients fasted for ≥4 hours and were scanned on a PET-MRI scanner (Biograph mMR, Siemens). The mean ± standard deviation injected dose of $^{11}$C-MET was 186 ± 60 MBq (5 ± 1.6 mCi), and the PET evaluation was based on the summed PET data obtained between 20 and 40 minutes after injection. The PET images were reconstructed iteratively using 3D ordinary Poisson-ordered subsets expectation maximization algorithm, incorporating the system point spread function with 3 iterations of 21 subsets. Data correction (normalization, attenuation,[22] and scatter correction) was fully integrated within the reconstruction process. A Gaussian postreconstruction filtering (FWHM = 2 mm) was applied.

The following MRI sequences were obtained: T1-weighted images (T1WIs) turbo spin echo (T1 TSE), T1WI magnetization-prepared rapid gradient echo without and with contrast enhancement (T1WI + CE), T1 susceptibility-weighted imaging, T2-weighted images (T2WIs) fast spin echo (T2 FSE), T2WI fluid-attenuated inversion recovery, T2 diffusion-weighted images from which the ADC maps were computed, and DIXON used to create the μ-map for attenuation correction of PET images.

### PET-MRI Image Analysis

The image quality was first visually assessed using a binary scale (interpretable vs noninterpretable). For noninterpretable PET images, additional postprocessing was performed to reduce motion artifacts using a list-mode–based motion correction approach.[23]

For PET images, the lesion uptake was visually assessed as increased, equivalent, or decreased, relatively to a contralateral normal-appearing brain region. The threshold to define the 3D tumor volume, according to the guidelines, was SUVs >1.3 of the mean value of a healthy-appearing brain, as measured in a spherical 1 $cm^3$ volume of interest including white and gray matter, measured at the level of the centrum semiovale.[5] $SUV_{max}$ and $SUV_{mean}$, as

**TABLE 1.** Grading, Anatomopathological Finding, and Molecular Analysis of the Lesions

| Patient ID | Pathological Findings | WHO Grade | KIAA1549-BRAF Fusion | BRAF V600E Mutation | Molecular Subgroup | MYC Amplification | TP53 Mutation |
|---|---|---|---|---|---|---|---|
| 1 | Pilocytic astrocytoma | 1 | Yes | No | NA | NA | No |
| 2 | CNS embryonal tumor with PLAGL amplification | NA | NA | No | NA | NA | No |
| 3 | Schwannoma | 1 | NA | NA | NA | NA | NA |
| 4 | Pilocytic astrocytoma | 1 | Yes | No | NA | NA | No |
| 5 | Pilocytic astrocytoma | 1 | Yes | No | NA | NA | No |
| 6 | Pilocytic astrocytoma | 1 | No | No | NA | NA | No |
| 7 | Ganglioglioma | 1 | No | No | NA | NA | No |
| 8 | Pilocytic astrocytoma | 1 | Yes | No | NA | NA | No |
| 9 | Medulloblastoma | 4 | NA | ND | Wnt | No | Yes |
| 10 | Medulloblastoma | 4 | NA | ND | Non-Wnt/non-Shh (group 3) | No | No |

NA, not applicable; ND, not done.

well as the metabolic tumoral volume (MTV), were calculated from this volume. Calculation of tumor-to-background ratios (TBRs) was performed as previously described.[6]

Regarding MRI, a visual analysis was performed. The maximal transverse diameter of the enhancing lesions was recorded using T1WI + CE, and the lesion enhancement was qualitatively graded as absent, moderate, or intense. The diffusion measurements were performed on coregistered PET-MRIs as previously described.[18] The $ADC_{min}$ was computed by placing an 8-mm diameter circular region of interest (ROI) on the ADC map in the region corresponding to the lesion $SUV_{max}$. It was then assessed whether this ROI corresponded to minimum $ADC_{min}$ as follows: the ROI was systematically moved outside the previously defined ROI in all the tumors to measure regions with significative lower diffusion. Careful attention was given to avoid blood vessels, necrosis, and hemorrhage.

### Histopathological and Molecular Analysis

An integrated diagnosis of each tumor, combining histological and molecular data, was performed by an experienced neuropathologist, according to the 2021 World Health Organization (WHO) classification.[24]

### Statistical Analysis

Descriptive statistics were performed (mean and range). The Spearman rank correlation coefficient was used to assess the correlation between CE and $SUV_{max}$; the Pearson correlation coefficient was used to assess the correlation between $ADC_{min}$ and $SUV_{max}$, as well as between MTV and lesion diameter measured on MRI, with 95% confidence interval (CI). Analyses were performed using the statistical software R, version 4.1.0 (R Foundation for Statistical Computing, Vienna, Austria).

## RESULTS

### Patient Characteristics

A total of 10 patients were included, the mean age was 8.9 years (range, 5–16), and 8 were male. At diagnosis, the clinical characteristics of the patients were headache (n = 4), vomiting (n = 3), cerebellar syndrome (n = 2), visual disturbance (n = 2), and hydrocephalus (n = 7). Performance status was (Lansky scale score) 100 for n = 3 and <100 for n = 7.

The pathological findings were as follows: pilocytic astrocytoma (n = 4), medulloblastoma (n = 2), ganglioglioma (n = 1), central nervous system (CNS) embryonal tumor (with *PLAGL* amplification; entity not yet included in the 2021 WHO classification, n = 1), and schwannoma (n = 1; Table 1).

All patients were alive at last follow-up, and the mean follow-up was 30 months (range, 23–44; Table 2).

### Image Analysis

In 9 patients, both PET and MRI were interpretable; for 1 patient, images were initially not interpretable due to head movement during image acquisition, but after motion correction, PET images were interpretable. Overall, 100% of PET images and 90% of MRIs were interpretable.

### MRI

The mean maximal diameter was 45.8 mm (range, 23–76). All lesions had T1 hyperintensity, as well as T2 and fluid-attenuated inversion recovery hyperintensities. They all presented contrast enhancement with various intensity, and only 2 had ADC restriction. The mean $ADC_{min}$ value was $0.98 \times 10^{-3}$ $mm^2/s$ (range, 0.40–1.39; Table 3).

### MET PET

All lesions visually presented an increased uptake of MET compared with background levels. In the normal-appearing brain region, the mean $SUV_{max}$ value was 1.0 (range, 0.8–1.4) and the mean $SUV_{mean}$ value was 0.7 (range, 0.6–1.1). In the lesion ROI, the mean $SUV_{max}$ value was 2.9 (range, 1.7–4.2) and the mean $SUV_{mean}$ value was 2.1 (range, 1.3–3.3). The mean MTV was 29.2 mL (range, 0.9–48.3; Table 4).

### $ADC_{min}$ and $SUV_{max}$

In 78% (n = 7/9) lesions, the ROI selected for ADC in the PET hot spot area corresponded to the minimum ADC value. A moderate negative correlation was found between $ADC_{min}$ and $SUV_{max}$ values (−0.39; 95% CI, −0.84 to 0.37; Fig. 1A).

### MTV and Lesion Maximal Diameter

The values of MTV and diameter of the enhancing lesions are plotted for each lesion in Figure 1B. A moderate positive correlation was found between MTV and maximal diameter values (0.34; 95% CI, −0.37 to 0.80).

### $SUV_{max}$ and CE

$SUV_{max}$ values and enhancement grade are plotted for each lesion in Figure 1C. The mean $SUV_{max}$ for strong enhancement was 2.6 (range, 2.1–3.2), and the mean $SUV_{max}$ for moderate enhancement was 3.5 (range, 2.6–4.7). There was no correlation

**TABLE 2.** Clinical Management Details and Outcome

| Patient ID | Surgery | Treatment Plan | FU Time, mo | FU Results |
|---|---|---|---|---|
| 1 | Incomplete | Surgery + CT | 44 | SD |
| 2 | Complete | Surgery + CT + RT | 42 | CR |
| 3 | Incomplete | Surgery alone | 40 | SD |
| 4 | Complete | Surgery alone | 36 | CR |
| 5 | Complete | Surgery alone | 34 | CR |
| 6 | Incomplete | Surgery alone then CT for progression | 33 | SD |
| 7 | Complete | Surgery alone | 32 | CR |
| 8 | Complete | Surgery alone | 28 | CR |
| 9 | Complete | Surgery + CT + RT | 24 | CR |
| 10 | Incomplete | Surgery + CT + RT | 23 | CR |

FU, follow-up; SD, stable disease; CR, complete response; CT, chemotherapy; RT, radiotherapy.

**TABLE 3.** Description of the MRI Findings

| Patient ID | Pathological Findings | Diameter, mm | Mean Enhancement | ADC Restriction | $ADC_{min}$ |
|---|---|---|---|---|---|
| 1 | Pilocytic astrocytoma | 46 | Strong | No | 1.156 |
| 2 | CNS embryonal tumor with PLAGL amplification | 62 | Moderate | No | NA |
| 3 | Schwannoma | 40 | Strong | No | 0.909 |
| 4 | Pilocytic astrocytoma | 32 | Moderate | No | 1.204 |
| 5 | Pilocytic astrocytoma | 76 | Strong | No | 1.393 |
| 6 | Pilocytic astrocytoma | 37 | Strong | No | 1.215 |
| 7 | Ganglioglioma | 23 | Mild | No | 0.652 |
| 8 | Pilocytic astrocytoma | 63 | Moderate | No | 1.289 |
| 9 | Medulloblastoma | 42 | Moderate | Yes | 0.4 |
| 10 | Medulloblastoma | 37 | Moderate | Yes | 0.588 |

NA, not available.

between $SUV_{max}$ according to the enhancement intensity (−0.15; 95% CI, −0.71 to 0.53). The $^{11}$C-MET PET and T1W CE MRI findings are reported in Figure 2. Patient 6 (Fig. 2A) presented a WHO grade 1 pilocytic astrocytoma. The lesion had a mild MET uptake associated with a strong heterogeneous contrast enhancement. Patient 9 (Fig. 2B) presented a WHO grade 4 Wnt-activated medulloblastoma. Conversely to the WHO grade 1 pilocytic astrocytoma, the lesion presented a more intense and homogeneous MET uptake but a mild heterogeneous contrast enhancement.

## Molecular and Histopathological Data Versus MET Uptake Parameters

The mean $SUV_{max}$ in WHO grade 4 lesions was 3.8 (range, 3.3–4.2) versus 2.5 (range, 1.7–3.0) in grade 1 lesions. The mean $TBR_{max}$ in grade 4 lesions was 4.1 (range, 3.5–4.7) versus 2.5 (range, 1.5–3.2) in grade 1 lesions. The mean $TBR_{mean}$ in grade 4 lesions was 5 (range, 4.1–5.8) versus 2.5 (range, 1.4–3.8) in grade 1 lesions. The mean $SUV_{mean}$ in grade 4 lesions was 2.8 (range, 2.2–3.3) versus 1.8 (range, 1.3–2.4) in grade 1 lesions. The mean MTV in grade 4 lesions was 22.0 (range, 18–26) versus 27.2 (range, 0.9–48.3) in grade 1 lesions. Among the subgroup with interpretable MRI, the mean $ADC_{min}$ in WHO grade 4 lesions was 0.5 (range, 0.4–0.6) versus 1.2 (range, 0.7–1.4) in grade 1 lesions.

Regarding the status of the KIAA1549-BRAF fusion, when present, the mean $SUV_{max}$ was 2.7 (range, 2.4–3) versus 2 (range, 1.7–2.3), and when absent, the mean $TBR_{max}$ was 2.7 (range, 2.1–3.2) versus 2 (range, 1.5–2.4), and the mean MTV was 30.9 (range, 11.0–48.3) versus 16.4 (range, 0.9–31.9).

## DISCUSSION

The present study reported that, although high-grade lesion may show heterogeneous conventional MRI features, in WHO grade 4 tumors herein, the level of MET uptake was higher, and ADC values were lower than in WHO grade 1 tumors, which agrees with previous studies.[25–29] Moreover, a meta-analysis focusing on glioma grading using $^{11}$C-MET PET in adults found a sensitivity of 94% and a specificity of 89% to differentiate low- from high-grade glioma.[30] This clinical indication is underlined in the EANM/EANO/RANO guidelines for adult patients,[5] as a negative scan excludes a grade 3/4 glioma, but it can also exclude a lymphoma or metastasis. However, grade 1/2 astrocytoma cannot be excluded since approximately 30% exhibit low uptake. As previously reported,[27] pilocytic astrocytoma, a low-grade tumor, had a high MET uptake herein, only slightly lower compared with that of the high-grade tumors. Thus, MRI features, especially the ADC value, which is high in pilocytic astrocytoma,[29] should be carefully evaluated and integrated to interpret MET uptake, taking into account the complementary information provided by PET and MRI.

Combined $^{11}$C-MET PET and MRI is used in brain tumors to perform targeted biopsies and to define the tumor limit[8,17]; the complementary information provided by MRI and PET parameters in pediatric brain tumors was assessed by a limited number of studies, and none used MET.[7,18,31] Herein, the MET uptake was compared with the $ADC_{min}$, which is used as a marker of dense tissue with high cellularity, small extracellular space, and high nuclear/cytoplasmic ratio.[32,33] A moderate negative correlation was found between these parameters, which could indicate a potential additional predictive value, as reported by Morana et al[18] using DOPA. As in the present study, they found a negative correlation between $ADC_{min}$ and DOPA

**TABLE 4.** Description of the Quantitative PET Finding

| Patient ID | Pathological Findings | $SUV_{max}$ | $TBR_{max}$ | $SUV_{mean}$ | $TBR_{mean}$ | MTV |
|---|---|---|---|---|---|---|
| 1 | Pilocytic astrocytoma | 3.0 | 2.7 | 2.4 | 3.4 | 39 |
| 2 | CNS embryonal tumor with PLAGL amplification | 4.1 | 3.3 | 3.3 | 4.6 | 57.6 |
| 3 | Schwannoma | 2.9 | 3.2 | 2.3 | 3.8 | 34 |
| 4 | Pilocytic astrocytoma | 2.4 | 3.2 | 1.4 | 2.4 | 25.2 |
| 5 | Pilocytic astrocytoma | 2.9 | 2.1 | 1.8 | 1.7 | 11 |
| 6 | Pilocytic astrocytoma | 2.3 | 2.4 | 1.3 | 1.9 | 31.9 |
| 7 | Ganglioglioma | 1.7 | 1.5 | 1.4 | 1.4 | 0.9 |
| 8 | Pilocytic astrocytoma | 2.4 | 2.6 | 1.9 | 2.9 | 48.3 |
| 9 | Medulloblastoma | 3.3 | 3.5 | 2.2 | 4.1 | 26 |
| 10 | Medulloblastoma | 4.2 | 4.7 | 3.3 | 5.8 | 18 |

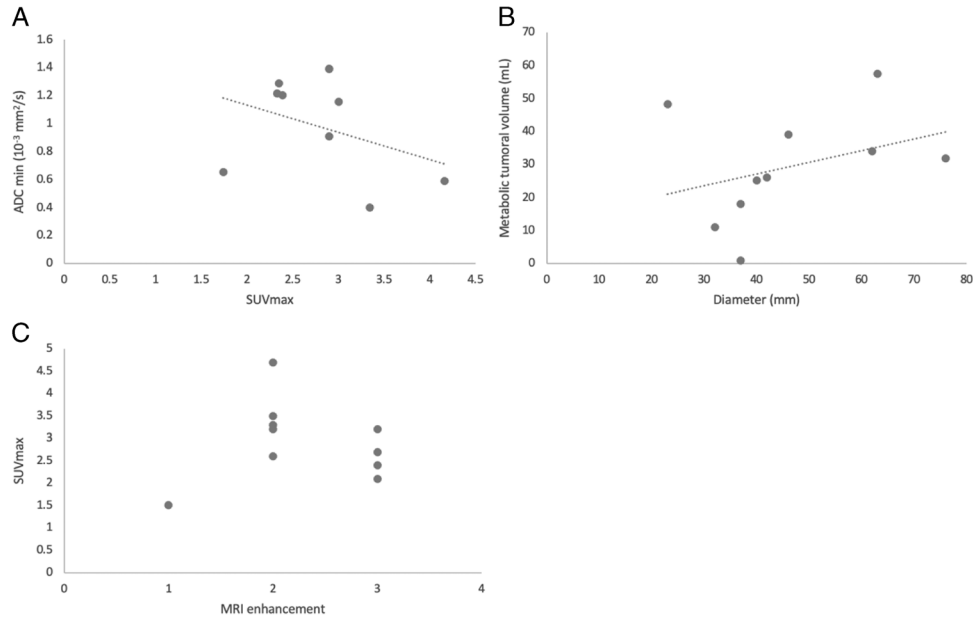


**FIGURE 1.** Comparison of PET and MRI parameters. **A**, Plot displays the $ADC_{min}$ according to the $SUV_{max}$. **B**, Plot displays the MTV according to the diameter measured on the MRI. **C**, Plot displays the $SUV_{max}$ according to the MRI enhancement.

uptake in 26 (mainly supra tentorial) astrocytic gliomas (Spearman $\rho = -0.76$, $P < 0.001$). Other studies used non–amino acid tracers, such as choline[7] or FDG,[31] that also partially reflect proliferation, and a negative correlation with $ADC_{min}$ was also found.

The present study found no correlation between MET uptake and CE intensity. CE reflects the blood-brain barrier disruption, but MET PET uptake reflects the L-type amino acid transporter 1 expression[34]; hence, the MET uptake provides additional information to the CE MRI, with clinical implication. For example, in addition to conventional CE MRI that might be negative, baseline $^{11}$C-MET PET is particularly useful to characterize low-grade glioma.[35] Moreover, in pediatric high-grade glioma, it delineates the non–contrast-enhancing tumor regions, which are at increased risk for recurrence.[36]

The present study has several limitations. The sample size was small, but pediatric brain tumors are rare,[37] and patients were prospectively included. In addition, the $^{11}$C-MET tracer was used, but due to the short half-life of $^{11}$C, an onsite cyclotron was required, which is rarely available in clinical practice. However, alternative $^{18}$F amino acid tracers such as $^{18}$F-FET and $^{18}$F-DOPA are available,[5,6] and $^{18}$F-FDG could also be useful.[6] In the present study, MRS was not included, whereas it is a valuable tool to improve the diagnostic performance of MRI in pediatric brain tumors.[38] Compared with $^{18}$F-DOPA, MRS was better to distinguish diffuse brain gliomas from nonneoplastic lesions, but $^{18}$F-DOPA uptake was better to differentiate low-grade from high-grade glioma.[4] In addition, in pediatric diffuse midline gliomas, $^{18}$F-DOPA PET but not MRS was able to distinguish H3K27M mutant from wild type.[19] These studies underline the complementary information provided by MRS and amino acid PET. Moreover, as a perspective, PET could be used to guide MRS during PET-MRI acquisition as reported for optimal voxel placement in adults.[39,40]

Larger multicenter studies are now required to confirm these preliminary findings, using simultaneous PET-MRI to provide a "one-stop shop" examination[41] and to avoid the radiation exposure of CT.[42] It is

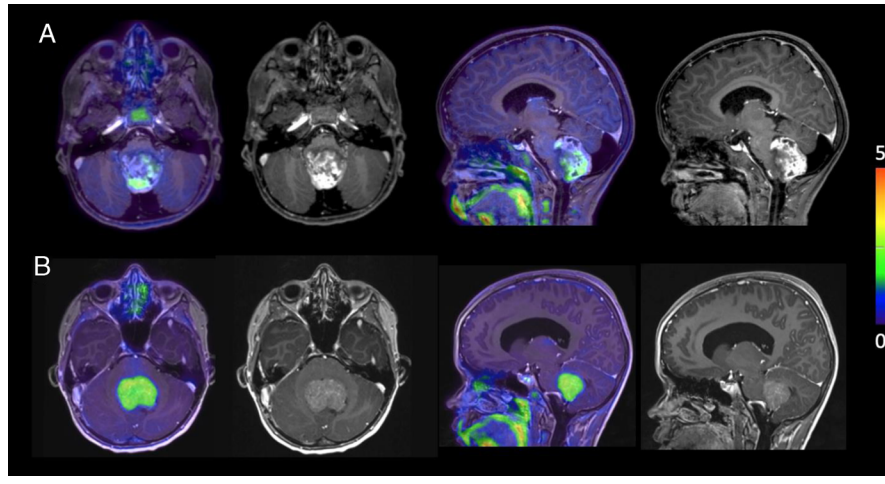


**FIGURE 2.** Axial and sagittal $^{11}$C-MET PET fused with T1W CE MRI images, respectively, depicts (**A**) a pilocytic astrocytoma (patient 6) and (**B**) a medulloblastoma (patient 9).

necessary to evaluate the potential use of $^{11}$C-MET as a biomarker at initial diagnosis and follow-up, as well as its potential predictive value, to support the use of targeted therapy and improve the quality of life of children.

## CONCLUSIONS

The present study suggests that preoperative $^{11}$C-MET PET-MRI for pediatric infratentorial tumors provides information complementary to that provided by MRI alone. To confirm these preliminary results, larger multicenter studies are needed. Potentially, PET-MRI might be able to provide sufficient information to characterize different tumor types, to avoid surgical procedure, and to help the oncological management to improve the overall survival and the quality of life of children.

## ACKNOWLEDGMENT

*The authors thank Shanez Haouari for the help in manuscript preparation.*

## REFERENCES

1. Jaremko JL, Jans LBO, Coleman LT, et al. Value and limitations of diffusion-weighted imaging in grading and diagnosis of pediatric posterior fossa tumors. *AJNR Am J Neuroradiol*. 2010;31:1613–1616.
2. Dhermain FG, Hau P, Lanfermann H, et al. Advanced MRI and PET imaging for assessment of treatment response in patients with gliomas. *Lancet Neurol*. 2010;9:906–920.
3. Pirotte B, Acerbi F, Lubansu A, et al. PET imaging in the surgical management of pediatric brain tumors. *Childs Nerv Syst*. 2007;23:739–751.
4. Morana G, Piccardo A, Puntoni M, et al. Diagnostic and prognostic value of $^{18}$F-DOPA PET and $^{1}$H-MR spectroscopy in pediatric supratentorial infiltrative gliomas: a comparative study. *Neuro Oncol*. 2015;17:1637–1647.
5. Law I, Albert NL, Arbizu J, et al. Joint EANM/EANO/RANO practice guidelines/SNMMI procedure standards for imaging of gliomas using PET with radiolabelled amino acids and [$^{18}$F]FDG: version 1.0. *Eur J Nucl Med Mol Imaging*. 2019;46:540–557.
6. Piccardo A, Albert NL, Borgwardt L, et al. Joint EANM/SIOPE/RAPNO practice guidelines/SNMMI procedure standards for imaging of paediatric gliomas using PET with radiolabelled amino acids and [$^{18}$F]FDG: version 1.0. *Eur J Nucl Med Mol Imaging*. 2022;49:3852–3869.
7. Fraioli F, Shankar A, Hargrave D, et al. $^{18}$F-fluoroethylcholine ($^{18}$F-Cho) PET/MRI functional parameters in pediatric astrocytic brain tumors. *Clin Nucl Med*. 2015;40:e40–e45.
8. Preuss M, Werner P, Barthel H, et al. Integrated PET/MRI for planning navigated biopsies in pediatric brain tumors. *Childs Nerv Syst*. 2014;30:1399–1403.
9. Veit-Haibach P, Ahlström H, Boellaard R, et al. International EANM-SNMMI-ISMRM consensus recommendation for PET/MRI in oncology. *Eur J Nucl Med Mol Imaging*. 2023;50:3513–3537.
10. Bailey DL, Antoch G, Bartenstein P, et al. Combined PET/MR: the real work has just started. Summary report of the third international workshop on PET/MR imaging; February 17–21, 2014, Tübingen, Germany. *Mol Imaging Biol*. 2015;17:297–312.
11. Langen K-J, Galldiks N, Mauler J, et al. Hybrid PET/MRI in cerebral glioma: current status and perspectives. *Cancers (Basel)*. 2023;15:3577.
12. Schäfer JF, Gatidis S, Schmidt H, et al. Simultaneous whole-body PET/MR imaging in comparison to PET/CT in pediatric oncology: initial results. *Radiology*. 2014;273:220–231.
13. Hirsch FW, Sattler B, Sorge I, et al. PET/MR in children. Initial clinical experience in paediatric oncology using an integrated PET/MR scanner. *Pediatr Radiol*. 2013;43:860–875.
14. Beuriat P-A, Cristofori I, Gordon B, et al. The shifting role of the cerebellum in executive, emotional and social processing across the lifespan. *Behav Brain Funct*. 2022;18:6.
15. Beuriat PA, Cristofori I, Richard N, et al. Cerebellar lesions at a young age predict poorer long-term functional recovery. *Brain Commun*. 2020;2:fcaa027.
16. Pollack IF, Agnihotri S, Broniscer A. Childhood brain tumors: current management, biological insights, and future directions. *J Neurosurg Pediatr*. 2019;23:261–273.
17. Pirotte B, Goldman S, Dewitte O, et al. Integrated positron emission tomography and magnetic resonance imaging–guided resection of brain tumors: a report of 103 consecutive procedures. *J Neurosurg*. 2006;104:238–253.
18. Morana G, Piccardo A, Tortora D, et al. Grading and outcome prediction of pediatric diffuse astrocytic tumors with diffusion and arterial spin labeling perfusion MRI in comparison with $^{18}$F-DOPA PET. *Eur J Nucl Med Mol Imaging*. 2017;44:2084–2093.
19. Piccardo A, Tortora D, Mascelli S, et al. Advanced MR imaging and $^{18}$F-DOPA PET characteristics of H3K27M-mutant and wild-type pediatric diffuse midline gliomas. *Eur J Nucl Med Mol Imaging*. 2019;46:1685–1694.
20. Rose S, Fay M, Thomas P, et al. Correlation of MRI-derived apparent diffusion coefficients in newly diagnosed gliomas with [$^{18}$F]-fluoro-L-dopa PET: what are we really measuring with minimum ADC? *AJNR Am J Neuroradiol*. 2013;34:758–764.
21. Rheims S, Rubi S, Bouvard S, et al. Accuracy of distinguishing between dysembryoplastic neuroepithelial tumors and other epileptogenic brain neoplasms with [$^{11}$C]methionine PET. *Neuro Oncol*. 2014;16:1417–1426.
22. Koesters T, Friedman KP, Fenchel M, et al. Dixon sequence with superimposed model-based bone compartment provides highly accurate PET/MR attenuation correction of the brain. *J Nucl Med*. 2016;57:918–924.
23. Reilhac A, Merida I, Irace Z, et al. Development of a dedicated Rebinner with rigid motion correction for the mMR PET/MR scanner, and validation in a large cohort of $^{11}$C-PIB scans. *J Nucl Med*. 2018;59:1761–1767.
24. WHO Classification of Tumours Editorial Board. *World Health Organization Classification of Tumours of the Central Nervous System*. 5th ed. Lyon, France: International Agency for Research on Cancer; 2021.
25. Utriainen M, Metsahonkala L, Salmi TT, et al. Metabolic characterization of childhood brain tumors: comparison of $^{18}$F-fluorodeoxyglucose and $^{11}$C-methionine positron emission tomography. *Cancer*. 2002;95:1376–1386.
26. Kertels O, Krauß J, Monoranu CM, et al. [$^{18}$F]FET-PET in children and adolescents with central nervous system tumors: does it support difficult clinical decision-making? *Eur J Nucl Med Mol Imaging*. 2023;50:1699–1708.
27. Dunkl V, Cleff C, Stoffels G, et al. The usefulness of dynamic *O*-(2-$^{18}$F-fluoroethyl)-L-tyrosine PET in the clinical evaluation of brain tumors in children and adolescents. *J Nucl Med*. 2015;56:88–92.
28. Sörensen J, Savitcheva I, Engler H, et al. 3. Utility of PET and $^{11}$C-methionine in the paediatric brain tumors. *Clin Positron Imaging*. 2000;3:157.
29. Porto L, Jurcoane A, Schwabe D, et al. Differentiation between high and low grade tumours in paediatric patients by using apparent diffusion coefficients. *Eur J Paediatr Neurol*. 2013;17:302–307.
30. Katsanos AH, Alexiou GA, Fotopoulos AD, et al. Performance of $^{18}$F-FDG, $^{11}$C-methionine, and $^{18}$F-FET PET for glioma grading: a meta-analysis. *Clin Nucl Med*. 2019;44:864–869.
31. Zukotynski KA, Vajapeyam S, Fahey FH, et al. Correlation of $^{18}$F-FDG PET and MRI apparent diffusion coefficient histogram metrics with survival in diffuse intrinsic pontine glioma: a report from the pediatric brain tumor consortium. *J Nucl Med*. 2017;58:1264–1269.
32. Huisman TAGM. Diffusion-weighted imaging: basic concepts and application in cerebral stroke and head trauma. *Eur Radiol*. 2003;13:2283–2297.
33. Nikam RM, Yue X, Kaur G, et al. Advanced neuroimaging approaches to pediatric brain tumors. *Cancers (Basel)*. 2022;14:3401.
34. Okubo S, Zhen H-N, Kawai N, et al. Correlation of L-methyl-$^{11}$C-methionine (MET) uptake with L-type amino acid transporter 1 in human gliomas. *J Neurooncol*. 2010;99:217–225.
35. Ninatti G, Sollini M, Bono B, et al. Preoperative [$^{11}$C]methionine PET to personalize treatment decisions in patients with lower-grade gliomas. *Neuro Oncol*. 2022;24:1546–1556.
36. Lucas JT Jr., Serrano N, Kim H, et al. $^{11}$C-methionine positron emission tomography delineates non-contrast enhancing tumor regions at high risk for recurrence in pediatric high-grade glioma. *J Neurooncol*. 2017;132:163–170.
37. *Cancer Statistics Review, 1975–2015 - Previous Version - SEER Cancer Statistics Review [Internet]*. SEER. [cited 2023]. Available at: https://seer.cancer.gov/archive/csr/1975_2015/index.html. Accessed September 1, 2023.
38. Goo HW, Ra Y-S. Advanced MRI for pediatric brain tumors with emphasis on clinical benefits. *Korean J Radiol*. 2017;18:194–207.
39. Kim ES, Satter M, Reed M, et al. A novel, integrated PET-guided MRS technique resulting in more accurate initial diagnosis of high-grade glioma. *Neuroradiol J*. 2016;29:193–197.
40. Bumes E, Wirtz FP, Fellner C, et al. Non-invasive prediction of IDH mutation in patients with glioma WHO II/III/IV based on F-18-FET PET-guided in vivo $^{1}$H-magnetic resonance spectroscopy and machine learning. *Cancers (Basel)*. 2020;12:3406.
41. Marner L, Henriksen OM, Lundemann M, et al. Clinical PET/MRI in neurooncology: opportunities and challenges from a single-institution perspective. *Clin Transl Imaging*. 2017;5:135–149.
42. Yang ZL, Zhang LJ. PET/MRI of central nervous system: current status and future perspective. *Eur Radiol*. 2016;26:3534–3541.